参赛队员姓名：<u>夏闻迪</u>

中学：<u>上海平和学校</u>

省份：<u>上海</u>

国家/地区：<u>中国</u>

指导教师姓名：<u>吴骏</u>

指导教师单位：<u>上海平和学校</u>

论文题目：<u>A Liquid Bubble Falling in Another Fluid: A Two-Phase Flow Phenomenon</u>

　　本参赛团队声明所提交的论文是在指导老师指导下进行的研究工作和取得的研究成果。尽本团队所知，除了文中特别加以标注和致谢中所罗列的内容以外，论文中不包含其他人已经发表或撰写过的研究成果。若有不实之处，本人愿意承担一切相关责任。

参赛队员：　夏闻迪　　指导老师：　吴骏

2020 年　9 月　14 日

A Liquid Bubble Falling in Another Fluid: A Two-Phase Flow Phenomenon

Wendi Xia

ABSTRACT

Bubbles exist everywhere in daily life. However, such a common phenomenon involves complex mechanisms, and therefore has never been investigated thoroughly—the achievements of the studies are limited and unsatisfactory. In this article, the phenomenon of a bubble falling in another immiscible fluid (mostly its settling speed) was investigated. A series of experiments, in which bubbles emerging from a syringe falls inside a measuring cylinder filled another fluid, was performed. Fluids used in the experiment include ethanol solutions and rice bran oil; for rice bran oil, its temperature-dependent viscosity was approximated by a function, which was proved effective on other similar oils. The dependence of the settling speed of the bubble on the density difference between the bubble and the surrounding fluid, as well as on the temperature of the surrounding fluid, was measured. Finite-Element Modeling (FEM) simulations were then carried out to model these situations, and lead to results that agreed with the experiments. It also visualized the flow field and revealed more details of the two-phase flow that were not detectable by our devices. Furthermore, inspired by some previous formulae, quantitative equations were derived semi-analytically by modifying an approximate drag formula originally developed for a rigid object at moderate Reynolds numbers. The equations were validated by simulations under ideal conditions.

Keywords: bubble, liquid-liquid two-phase flow, viscosity

CONTENTS

I. INTRODUCTION

Two immiscible fluids often generate bubbles. From cooking to crude oil leakage, liquid bubbles exist everywhere in our daily life. Although numerous investigators have devoted themselves to this day-to-day phenomenon in the past century, calculating the settling speed of falling liquid bubbles has long been a concern. This dilemma is encountered not only in liquid bubbles, but also in solid and gaseous ones. Two major factors are involved in determining the settling speed: the body force of the bubble, and the drag force exerted on the bubble by the other fluid.

For very low Reynolds numbers, Stokes gave an analytical solution—using the Navier-Stokes equation—to calculate the drag force encountered by a solid sphere. However, flow fields with higher Reynolds number have different properties. Scientists have made empirical modifications to the equation, including Oseen's [1] and Goldstein's [2] efforts. But a perfect analytical equation, describing the drag coefficient and applicable in a wide range of Reynolds numbers, has never been developed.

Many scholars, including A. R. Khan and J. F. Richardson, claimed that "outside the region where Stokes' Law applies, a satisfactory theoretical form of this function does not exist. Therefore, it is necessary to apply some form of empirical treatment to correlate and interpret experimental data." [3]

This paper presents both experimental data and simulation results. The experimental data were collected through an experiment in which a liquid came out slowly from a metal needle immersed in a less dense liquid, formed a bubble and fell. The simulation results were obtained from FEM (finite element model). This was made possible by the nowadays developed software, while back in the era where computer technologies were not as sophisticated, such approach was not available to the pioneers in this field. In the simulation, the viscosity curve of the oil was approximated by a hyperbola. Detailed discussions will be presented in later sections.

The paper first examines the factors influencing the settling speed: density and viscosity. Then, it takes a close look at the patterns of the flow field in the model and analyzes various factors and phenomena impacting the drag force, such as speed gradients, vortexes, separation points. Finally, it investigates one of the most ancient but effective and commonly used empirical formulae describing the velocity of a falling rigid sphere. By analyzing the relationship between solid and liquid bubbles, the paper presents a new method to find a solid

equivalent for a liquid bubble. Thus, equations that are applicable to solid bubbles can be extended to liquid ones in a wide range of Reynolds numbers.

II. METHOD

A. *Experiment Setup*

The experiment involved a denser liquid coming out from a metal needle immersed in another liquid and forming a bubble. The bubble gradually increased until its gravity became greater than the buoyant force and the surface tensions clinging to the needle. The bubble then fell and accelerated until reaching its settling speed.

The experiment investigated the impact of the density difference and the temperature on the settling speed of the falling bubble.

Pump
(powered by a servo motor)

Injector containing a fluid
with density ρ

Metallic needle

Bubble with a
diameter of L

Outer fluid of density
ρ_0 and viscosity μ
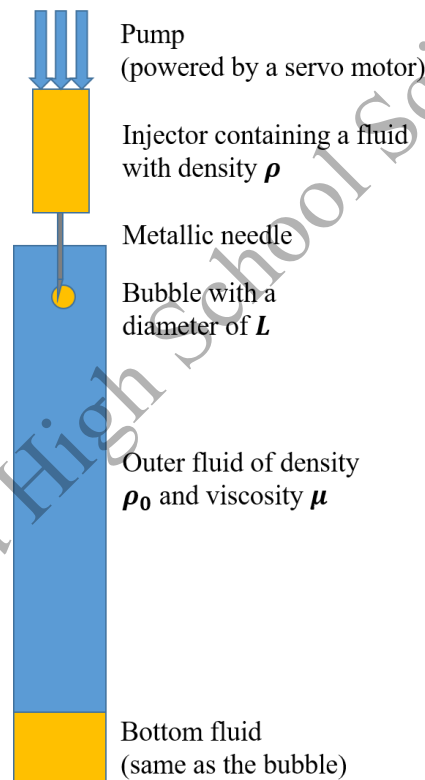
Bottom fluid
(same as the bubble)

Figure 1.   Front view of the experiment. The injector injects a bubble through a metallic needle into another fluid. The two colors, yellow and blue, mark the bubble fluid and the outer fluid, respectively.

The pump was placed on top of the cylinder and vertically, with the needle pointing at the center line of the measuring cylinder (see Figure 1). A tripod was used to support the pump. The tripod's height was carefully chosen so that the needle tip was $1cm$ below the uppermost line of the graduated cylinder, where the level of the other liquid would be. The pump was set to pump at a rate of $5mm \cdot s^{-1}$. The diameter of the tube in which the piston moved was $15mm$.

Therefore, the cross-sectional area was about $177mm^2$, and the liquid was ejected at a rate of $0.88mL \cdot s^{-1}$.
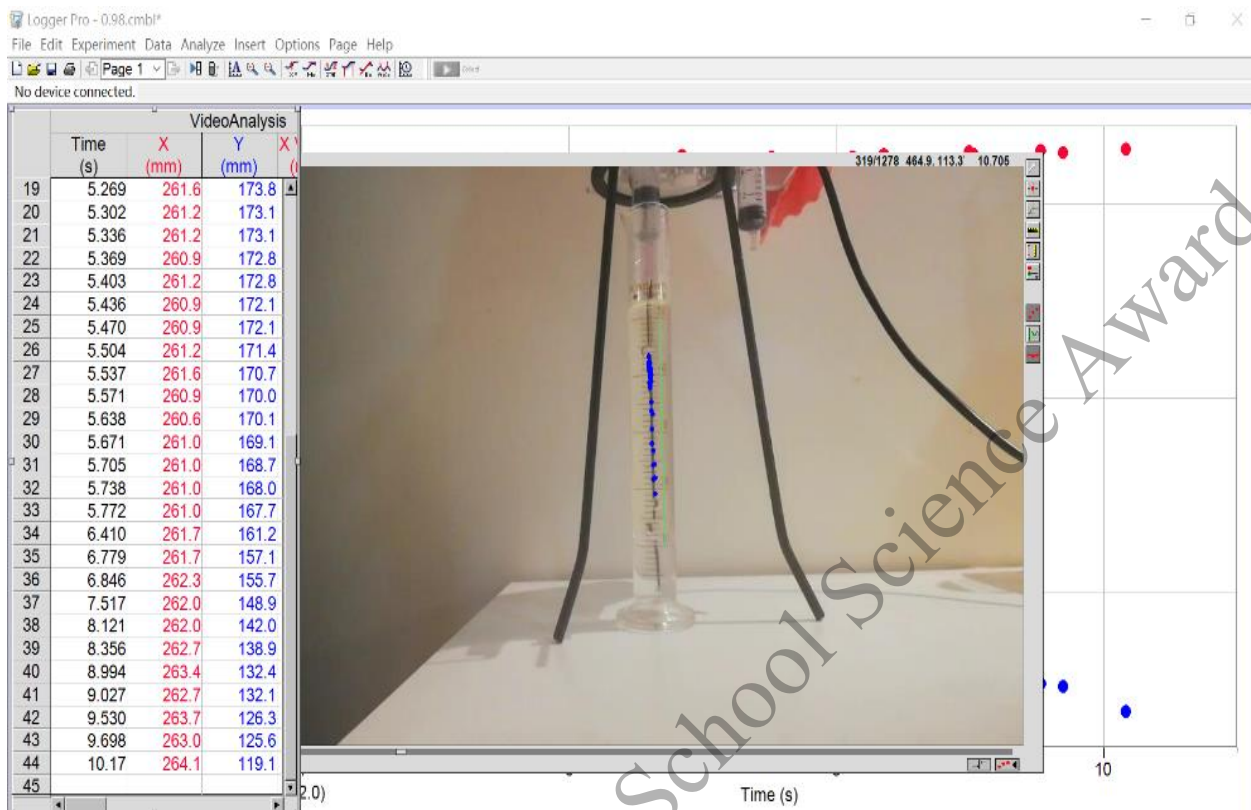

Figure 2.   Video Analysis with Logger Pro

The camera was placed around $35cm$ away from the cylinder. It filmed the falling process of the bubble. Using the video and the video analysis software, Logger Pro (see Figure 2), the height of the bubble (with respect to the lines on the cylinder) could be plotted in relation to time. The settling velocity of the bubble was then calculated and recorded.

For the investigation of density, another $100mL$ measuring cylinder and an electronic balance were applied to produce ethanol solutions of different concentration and thus different densities. Then, either the oil bubble was dropped into the ethanol solution (when the ethanol solution was less dense than the rice bran oil), or the ethanol solution bubble was dropped into the oil (when the ethanol solution was denser than the rice bran oil).

For the investigation of temperature, the measuring cylinder, filled with a little water at the bottom and the rice brand oil on top of it, was placed in a pot of hot water until being heated to the target temperature. An electronic thermometer was placed inside the cylinder to check the temperature. This method made it heat up uniformly, and prevented the water at the bottom from boiling and forming gaseous bubbles.

B. Simulation

1) Model

A finite element model was built in Comsol 5.4 to simulate the process of a bubble falling in another fluid.

The bubble fell along the center line of the cylinder, and the fluids were uniformly distributed in the cylinder. It was assumed that the velocity field was symmetric, without a Kármán vortex street. For simplicity, the model was axisymmetric, and this allowed a finer mesh to be set under a given amount of calculation.
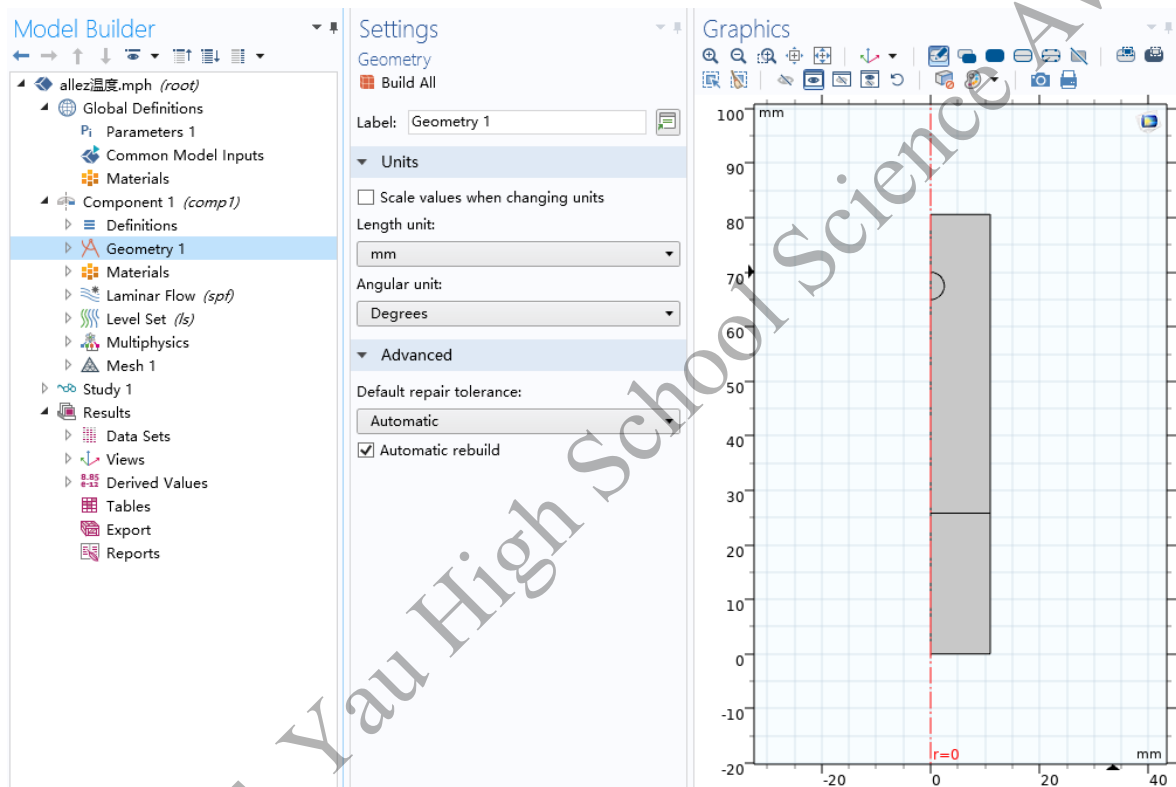

Figure 3.   Model Geometry: a rectangle representing the two fluids inside the cylinder, a line that marked the interface of the two fluids, and a circular liquid bubble.

The geometry of this model (see Figure 3) consisted of three parts: a rectangle representing the two fluids inside the cylinder, a line that marked the interface of the two fluids, and a circular liquid bubble. Due to surface tension, the shape of the bubble when it had just left the needle tip in the experiment was a sphere.

The width of the rectangle was $10.92mm$, equal to the radius of the measuring cylinder in the experiment. The height of the rectangle was less than the actual value. This was to include less nodes, simplifying the calculation. A test was run to show that the bubble, once reaching

its maximum speed, held that speed until it met the interface. Therefore, the distance between the bubble and the bottom did not affect its speed much.

The radius of the circle, representing the radius of the bubble, varied across experiments, but all the datapoints on the trend lines had bubble radii $2.5mm$. The mechanism of bubble radii changes will be viewed in the results section.

The material properties were manually assigned according to the actual value. However, there was not much literature value for the viscosity of rice bran oil, and an approximation was required. It will be shown in details in the next section.

Since only the settling speeds of the bubbles were recorded, the initial speed of the bubble set in the model does not affect the outcome. It was set to 0.

The upper and lower liquid surfaces were set as walls. The lower surface was a wall with no slip because the bottom of the measuring cylinder is solid. The upper surface was a wall with slip, ignoring air viscosity. The outside edge was set as a wetted wall because it was submerged in fluids in the experiment when the bubble came down.

The model involved the Earth's gravitational field. Thus, the gravitational constant was $g = 9.81m \cdot s^2$.

The model solved the Navier-Stokes equations for the conservation of momentum,

$$\frac{D\vec{V}}{Dt} = \vec{f} - \frac{1}{\rho}\nabla p + \frac{\mu}{\rho}\nabla^2\vec{V} + \frac{1}{3}\frac{\mu}{\rho}\nabla(\nabla \cdot \vec{V}) \tag{1}$$

and a continuity equation for the conservation of mass,

$$\frac{\partial \rho}{\partial t} + \nabla \cdot (\rho\vec{V}) = 0 \tag{2}$$

Here $\vec{V}$ is the velocity field, $\frac{D\vec{V}}{Dt}$ is the material derivative, t represents time, $\vec{f}$ is the body force, ρ is the density of the fluid, ∇ is the divergence, μ is the viscosity, and p is the pressure. The surface tension on the interface was included so that the geometry of the bubble would be accurately simulated. Without surface tension, the bubble would deform quickly.

2)   Approximation of the Viscosity of Rice Bran Oil

The available literature values, shown in Table I, only included the viscosities of rice bran oil under $26℃$, $38℃$ and $50℃$, measured by Diamante and Lan [4]. However, the viscosity

curves of some other similar cooking oils were also available, as shown in Table II, according to the study of Sahasrabudhe *et al.* [5]

TABLE I.   THE LITERATURE VISCOSITY OF RICE BRAN OIL

$T/°C$	$\mu_{RiceBranOil}/(Pa \cdot s)$
26	0.0593 ± 0.0006
38	0.0398 ± 0.0001
50	0.0280 ± 0.0000

TABLE II.   THE LITERATURE VISCOSITY OF CANOLA OIL AND OLIVE OIL

$T(°C)$	$\mu_{oil}(mPa \cdot s)$	
	Canola Oil	Olive Oil
22 ± 1	63.5 ± 1.6	74.1 ± 2.2
40	34.9 ± 0.9	40.1 ± 1.5
60	18.8 ± 0.3	21.1 ± 0.9
80	11.8 ± 0.4	13.4 ± 0.9
100	8.2 ± 0.4	9.6 ± 0.8
120	5.5 ± 0.2	6.1 ± 0.2
140	4.4 ± 0.1	4.8 ± 0.2
160	3.7 ± 0.2	4.0 ± 0.1
180	3.0 ± 0.2	3.3 ± 0.1
200	2.6 ± 0.3	

It was discovered that the following equation could be used to fit the viscosity curve of oils:

$$\mu = \frac{a_1}{T+a_2} + a_3 \tag{3}$$

Where T is the temperature, and k_1, k_2 and k_3 are constants specific to the type of oil.
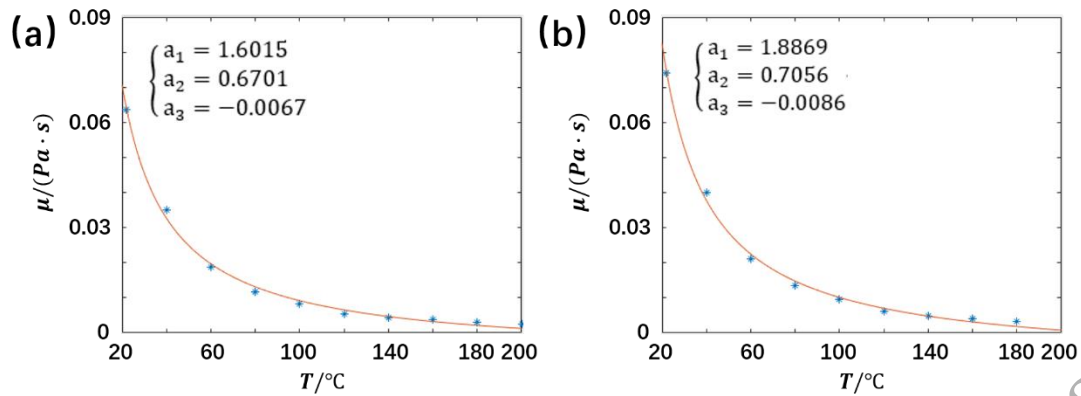
8

Figure 4.   Approximation of the viscosity of (a) canola oil and (b) olive oil. The blue asterisks are the literature values, and the orange lines are the fitting lines determined by Equation (3) and the parameters in the curly brackets.

Figure 4(a) shows the approximation of the viscosity of canola oil using Equation (3). The blue line represents the literature value, while the orange line is the line of best-fit. Figure 4(b) shows the approximation of olive oil. The error of the approximation is relactively low. Apply Equation (3) to rice bran oil, and the result is shown in Figure 5.
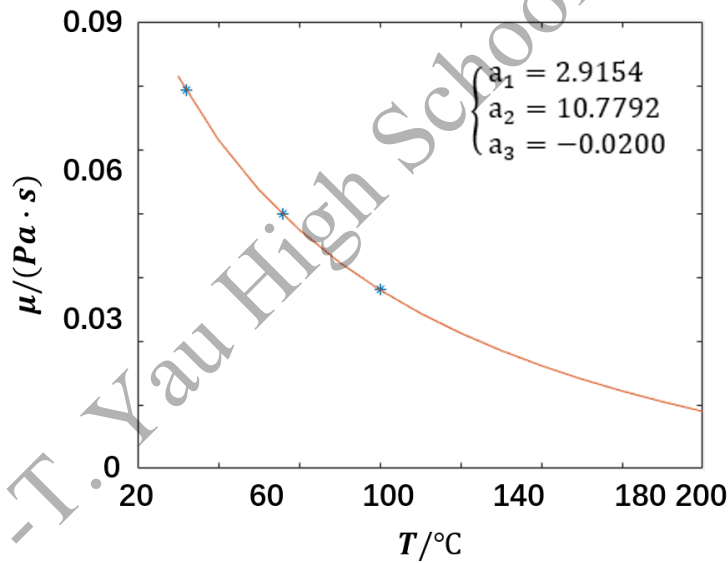

Figure 5.   Approximation of the viscosity of rice bran oil. The blue asterisks are the literature values at 26℃, 38℃ and 50℃, and the orange line is the best-fit line based on Equation (3).

The viscosity of rice bran oil is

$$\mu_{RiceBranOil} = \frac{2.9154}{T(\text{in}℃)+10.7792} - 0.0200 \tag{4}$$

III. RESULTS

In this section, we shall first review the basic theory of drag. We will then move on to discuss our experimental results.

A. Theories of drag of an object in fluid

The bubble reached its settling speed with the drag balanced with the bubble's body force. The body force F is defined as the difference between the bubble's weight and buoyant force.

$$F = W - \mathrm{F_{buoyant}} \tag{5}$$

where W is the weight of the bubble, and $\mathrm{F_{buoyant}}$ is the buoyant force. Therefore,

$$F = (\rho - \rho_0)Vg \tag{6}$$

where ρ is the density of the bubble, ρ_0 is the density of the outer fluid, V is the volume of the bubble, and g is the gravitational constant. Also, the drag force F_D of an object is given by Equation (7):

$$\mathrm{F_D} = \frac{1}{2}\rho_0 \mathrm{v}^2 \mathrm{C_D} A \tag{7}$$

Here v is the speed of the object, C_D is the drag coefficient, and A is the cross-sectional area.

The calculation of C_D is comparatively more complicated. For rigid bubbles, it depends solely on the Reynolds number, which is defined as

$$Re = \frac{\rho_0 \mathrm{vL}}{\mu} \tag{8}$$

Stokes obtained an analytical solution applicable for rigid bubbles at very small Reynolds numbers by solving the equation of Navier-Stokes. [6]

$$\mathrm{C_D} = \frac{48}{Re} \tag{9}$$

However, as mentioned before, liquid bubbles have internal flows. Equation (9) needs some modification to become applicable to non-rigid spheres: [7]

$$\mathrm{C_D} = \frac{24}{Re}\frac{2+3(\mu_D/\mu_C)}{3+3(\mu_D/\mu_C)} \tag{10}$$

Here μ_D is the viscosity of the spherical bubble and μ_C is the viscosity of the outer fluid. Note that here C_D is already multiplied by the coefficient of $\frac{1}{2}$ in Equation (7). Thus, for solid bubbles, Equation (10) coincides with Equation (9). Equation (10) is indeed a desirable approximation at low Reynolds numbers. "However, the experimentally obtained C_D values have shown different trends in variation with Re, which has encouraged many investigators to

propose various formulation for C_D." For higher Re, one of the most commonly used equation to calculate the drag coefficient of a rigid sphere was proposed by Schiller and Naumann: [8]

$$C_D = \frac{24}{Re}(1 + 0.15Re^{0.687}) \tag{11}$$

(For a rigid sphere with $0.2 < Re < 800$)

Same as Equation (10), here C_D is already multiplied by the coefficient of $\frac{1}{2}$ in Equation (7).

Also, for A in Equation (7) and V in Equation (6), since the bubble is a sphere,

$$A = \pi \left(\frac{L}{2}\right)^2 \tag{12}$$

$$V = \frac{4}{3}\pi \left(\frac{L}{2}\right)^3 \tag{13}$$

where L is the diameter of the bubble. In conclusion, when the bubble is in equilibrium,

$$F_D = F \tag{14}$$

Thus,

$$3\pi\mu vL \left[1 + 0.15\left(\frac{\rho_0 vL}{\mu}\right)^{0.687}\right] = \frac{4}{3}\pi \left(\frac{L}{2}\right)^3 (\rho - \rho_0)g \tag{15}$$

(For a rigid sphere with $0.2 < Re < 800$)

This section discusses the determinants of drag force and presented a detailed discussion of the equations obtained by prior investigators. Their equations successfully describe the drag force of a bubble at a low Reynolds number and the drag force of a solid bubble at a higher Reynolds number. However, the equation describing the settling speed of a liquid bubble at a higher Reynolds number is absent.

In the following sections, a qualitative analysis will be presented to show the impact of various factors on the settling speed of the liquid bubble. Then, based on that, a quantitative equation will be deduced.

B. Simulation and Experiment Results

1)   Vortex

It was discovered that there was a vortex behind oil bubbles. Figure 6(a) shows an ethanol solution bubble whose density was $930 kgm^{-3}$ falling through the oil, and Figure 6(b) shows an oil bubble falling through an ethanol solution with density 870kgm^{-3}. The reason was that, for the oil bubble, the Reynolds number was higher. The definition of the Reynolds number is shown in Equation (8).
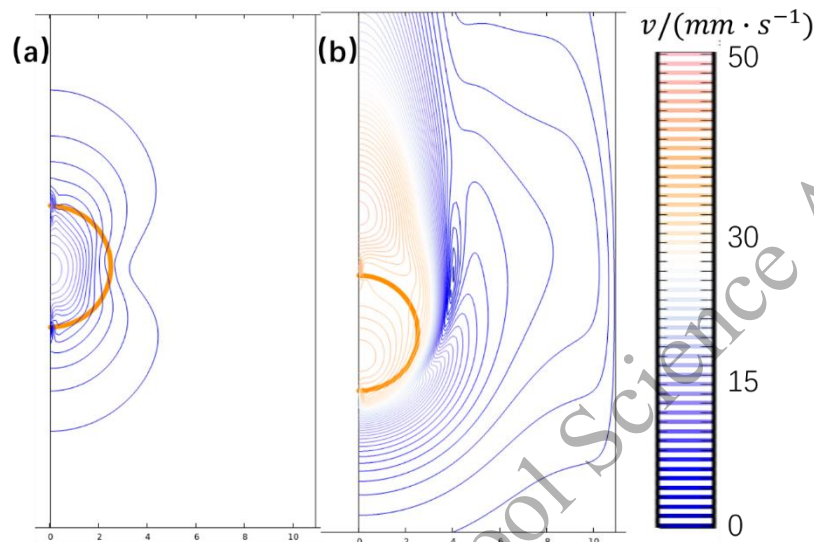

Figure 6.   The ethanol solution bubble (a) and the oil bubble (b) with a vortex behind. Contour: speed field; interval: $1 mm \cdot s^{-1}$

Under a relatively high Re, the fluid separated from the interface and created a vortex behind the bubble. According to Johnson and Patel [9], for a flow past a solid sphere, steady and symmetrical vortexes exist when Re exceeds 20. Also, asymmetrical but steady vortexes exist when $210 < Re < 270$. Afterwards, when $Re > 270$, the vortexes become unsteady. In the investigation of density, Re ranges from 0.2600 to 1.646 for ethanol bubbles and ranges from 89.31 to 368.2 for oil bubbles. Therefore, all the oil bubbles had vortexes behind them, while all the ethanol bubbles did not. Note that when $Re > 270$, the simulation only provided an approximation. In the investigation of temperature, Re was large enough to generate vortexes, but it never exceeded 210, either in simulation or in the actual experiment.

2)   *Bubble Size*

The surface tensions of the bubble-outer fluid interface, the bubble-needle interface and the outer fluid-needle interface kept the bubble on the needle tip. When the bubble was large enough to overcome the surface tensions, the bubble fell.

The diameter of the bubble varied across experiments. However, the actual bubble diameter could hardly be measured because it was two orders of magnitudes less than the height of the measuring cylinder. The resolution of the video analysis application was not high enough

to determine the precise size of the bubbles. However, qualitative comparisons could still be made. Figure 7 shows the pictures captured by a separate camera. The length between two graduation lines on the measuring cylinder was $2.62mm$.

Water bubble

$$\begin{cases} \rho - \rho_0 = 100kg \cdot m^{-3} \\ T = 26°C \end{cases}$$

Heated up

$$\begin{cases} \rho - \rho_0 = 100kg \cdot m^{-3} \\ T = 90°C \end{cases}$$

Oil bubble

$$\begin{cases} \rho - \rho_0 = 90kg \cdot m^{-3} \\ T = 26°C \end{cases}$$

Less density difference

$$\begin{cases} \rho - \rho_0 = 10kg \cdot m^{-3} \\ T = 26°C \end{cases}$$
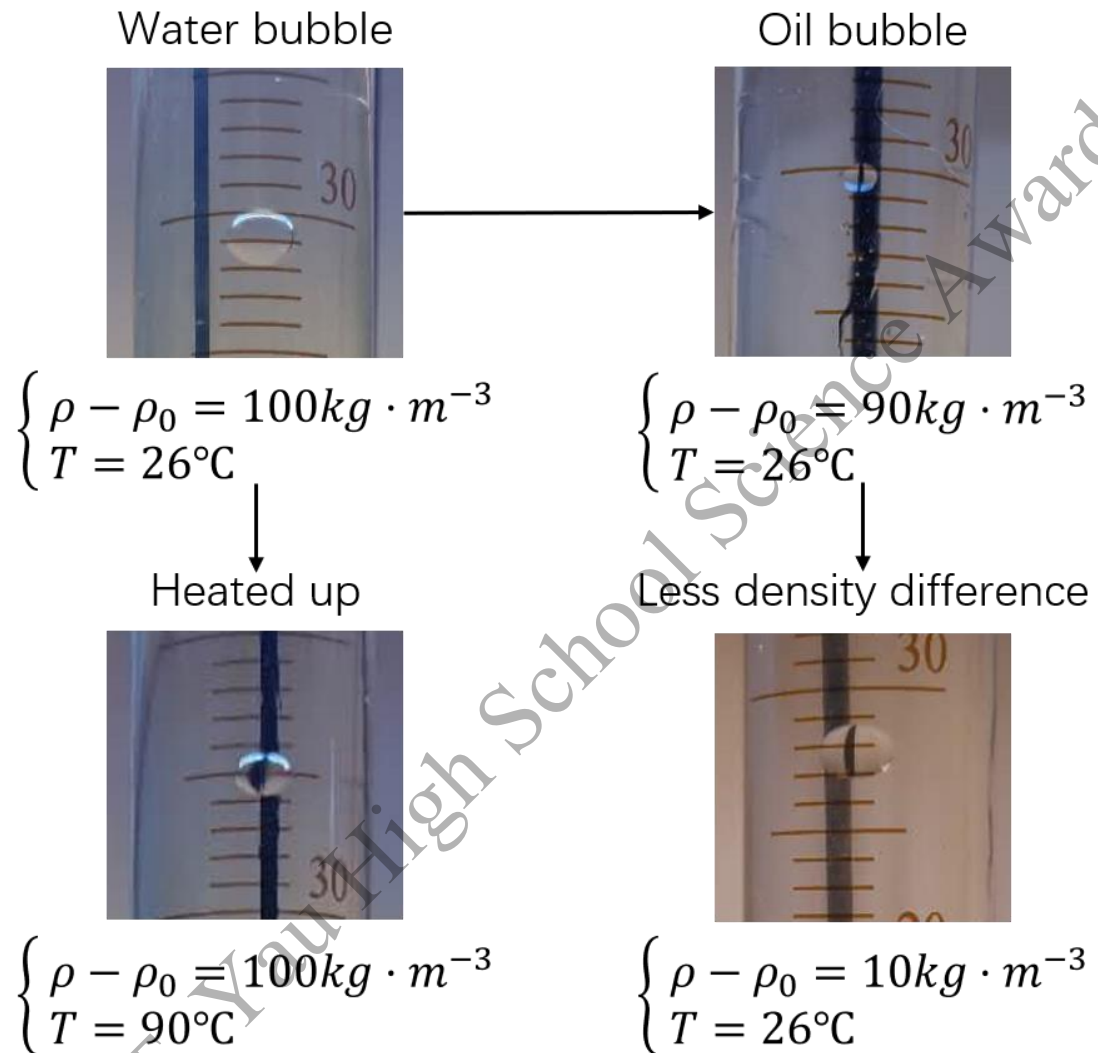
Figure 7.   Water and Oil bubbles under different density differences and temperatures. The length between two graduation lines on the measuring cylinder was $2.62mm$.

Due to refraction, the images of the bubbles are horizontally stretched, but their vertical lengths do not change.

The first column of Figure 7 suggests that the water bubble became smaller as the temperature increases. This was because the temperature negatively impacted the surface tensions. However, the impact was comparatively insignificant. The second column shows that the diameter increased as the density difference decreases. As the density ratio decreased, the bubbled had to be increasingly large to overcome the surface tensions. Also, the first row shows

that, in the experiment, the oil bubbles were much smaller than ethanol solution bubbles, *ceteris paribus*.

Since the diameters of water bubbles under different temperatures were approximately two intervals ($5.24mm$) long, the bubble diameters in the simulations were always 5mm. It was a potential source of error, and its impact will be discussed.
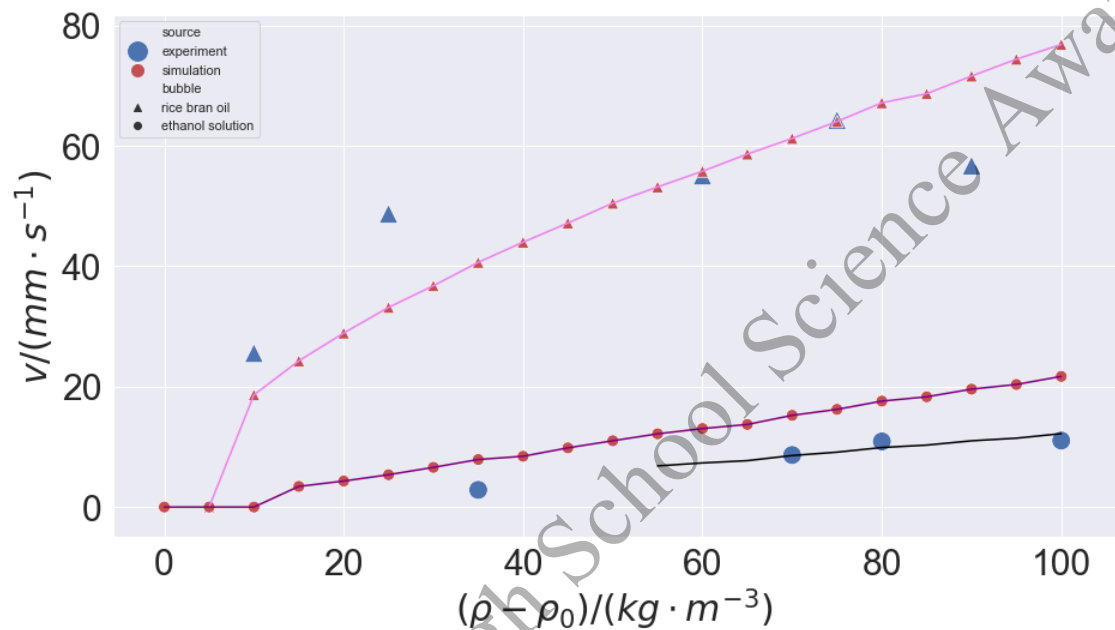
3)   The Impact of Density

Figure 8.   Settling speed as function of density difference, when rice bran oil bubbles fall in ethanol solutions (triangles) and when ethanol solution bubbles fall in the oil (dots.) Red markers for the simulations and blue markers for the experiments. The black line is the simulation results after calibration.

In Figure 8, the vertical speed of the bubble is plotted in relation to the density difference of the bubble to the surrounding fluid. The blue datapoints represent the data acquired through experiments, while the red datapoints represent the simulation results. All the simulation results were acquired with a bubble diameter L of $5mm$. Dots indicated that the bubbles consisted of ethanol solution, while triangles indicated that the bubbles were rice bran oil.

The datapoints on the x-axis mark the situations where the bubble suspended in the surrounding fluid or fell at undetectable speed.

Both trendlines increased as density difference increased. This is because the body force F is proportionate to $(\rho - \rho_0)$, while the drag force is constant when ρ_0, v and L are constant.

The trendline of oil bubbles slightly concaves down when the density ratio is between 1.01 and 1.06, and becomes almost linear thereafter. However, the experimental data concaved down

much more. when $\rho - \rho_0 > 60$, Re exceeds 270, so some inaccuracy is comprehensible. However, this is also because that the bubble diameter L decreased as the density difference $(\rho - \rho_0)$ increased in the actual experiment. According to Equation (7), the drag force F_D is proportional to L if C_D is constant. However, the body force F of the bubble was proportional to L^3. A larger radius would therefore result in a higher vertical speed. As the density difference increased, the size of the bubble decreased, so that its vertical velocity did not increase as rapid as the simulated trendline, which held L constant. Simulation shows that, when oil bubbles fall in an ethanol solution with density $875\text{kg} \cdot \text{m}^{-3}$, a bubble 6mm in diameter is $4.178mm \cdot s^{-1}$ faster than a bubble 5mm in diameter.

The trendline of ethanol solution bubbles increased almost linearly. The experimental values exhibited similar behavior, only that it concaved down slightly, which was explained in the previous paragraph. Note that the simulated datapoints were consistently below the trendline, which was probably caused by an error in bubble radius measurement, rice bran oil viscosity data, or a systematic error in the simulation. However, the trend of the lines still matches closely.

It is suspected that the error was caused by the literature value of rice bran oil viscosity. The settling speed of an ethanol bubble would be severely affected but that of an oil bubble would not, if the oil had a different viscosity as the literature value, since the drag mainly came from the viscous force of the outer fluid. This, however, is very likely, given the difference in ingredients and processing across different kitchen oil manufacturers. The black line represents the simulation results after calibration. This hypothesis will be validated in the investigation of temperature.

Also, the oil bubble trendline is higher than the ethanol solution bubble trendline. Apart from the difference in ρ_0, which directly impacted the drag, it should be attributed to the impact of viscosity.

4)   The Impact of Temperature and Viscosity

This section studies the impact of viscosity of the outer fluid on the terminal speed of the bubble. The most convenient way to change the viscosity of a fluid is usually changing the temperature. Therefore, in the experiment, water bubbles fell in rice bran oils with different temperatures, and their settling speeds were recorded (see Figure 9). The simulations held the densities constant.
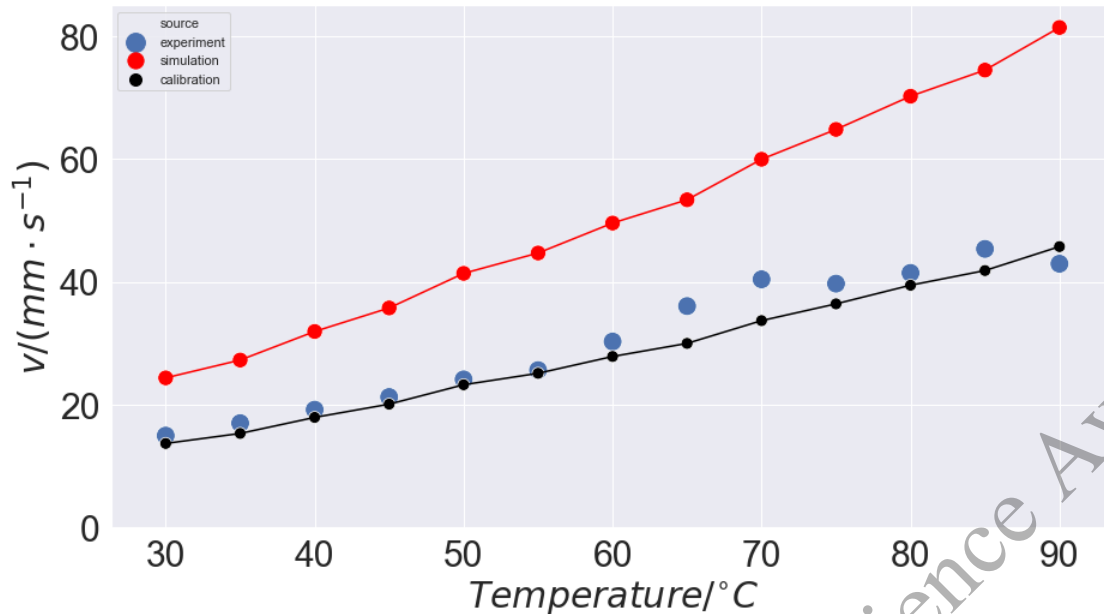
Figure 9.   Settling Speed of water bubble falling in oil as a function of temperature. The blue dots are experimental values, while the red line and the black line are the simulation results and the simulation results after calibration, respectively.

In Figure 9, the red datapoints represent simulation results, while the blue datapoints represent experimental values. Both of the lines increase as temperature increases and oil viscosity decreases.

Meanwhile, the simulation results are always greater than the experimental results. Suppose that the error is systematic and caused by the inaccuracy in the literature values of the viscosity of rice bran oil, which is a hypothesis mentioned before in the investigation of density. Thus, the simulation results can be calibrated by multiplying a coefficient. It is worth mentioning that the calibration is only valid when the changes in Reynolds number and the internal flow of the bubble are negligible, according to Equation (15)—when the Reynolds number is constant, C_D is constant; when the internal flow field of the bubble does not change, the liquid bubble can be analogized with a solid bubble (further discussions will be presented later,) so that Equation (15) is applicable.

The coefficient is determined by averaging the ratios of experimental results to simulation results in Figure 8 whose $(\rho - \rho_0) = 70, 80$ and $100 \text{kg} \cdot m^{-3}$; they, too, represent the settling speed of an oil bubble, and they have similar Reynolds numbers as the datapoints in Figure 8. The result is $\frac{1}{1.78}$. In Figure 8 and Figure 9, the black lines are the calibrated lines.

From $30°C$ to $60°C$, the calibrated line increases more rapidly than the experimental result. This is due to its constant, rather than decreasing, bubble radius.

16

From 60℃ to 70℃, the experimental result increases dramatically. This was possibly because the actual Reynolds number increased as μ decreases. Thus, C_D decreased. Another possible cause was that not only the scale but also the shape of the actual $\mu_{RiceBranOil} - T$ curve was different from the literature values.

From 70℃ to 90℃, the experimental values become almost flat. One of the possible causes was, in fact, a technical difficulty: since that in the experiment, the injector connected to the pump was plastic, the water could not be heated. The water bubble was at room temperature when it came into the hot oil. It cooled the surrounding oil down and increased oil viscosity. The second possible cause was the convection inside the measuring cylinder: in the experiment, the heated measuring cylinder was exposed in room temperature when the water bubbles fell through the oil. Therefore, the oil near the wall of the cylinder was cooler than the oil in the center. The cooler oil was denser and thus sank, while the warmer oil in the center rose. The water bubble falling through the center line met this resistant force and slowed down. However, in the simulation, the wall was insulated. The higher the oil temperature, the faster it would cool down, the stronger the convection.

In conclusion, the simulation results, especially those after calibration, are close to the results attained in the experiments. It proves the effectiveness and accuracy of the simulation.

IV. DISCUSSIONS

A. The Impact of Viscosities

To fit Equation (9) on liquid bubbles, Equation (10) focused on the viscosity ratio of the inner and outer fluids. This proved the viscosities of both fluids a vital factor in determining the settling speed of a liquid bubble. This section will dig deeper into exactly how the viscosity of the two fluids influence the falling speed of the bubble, respectively.
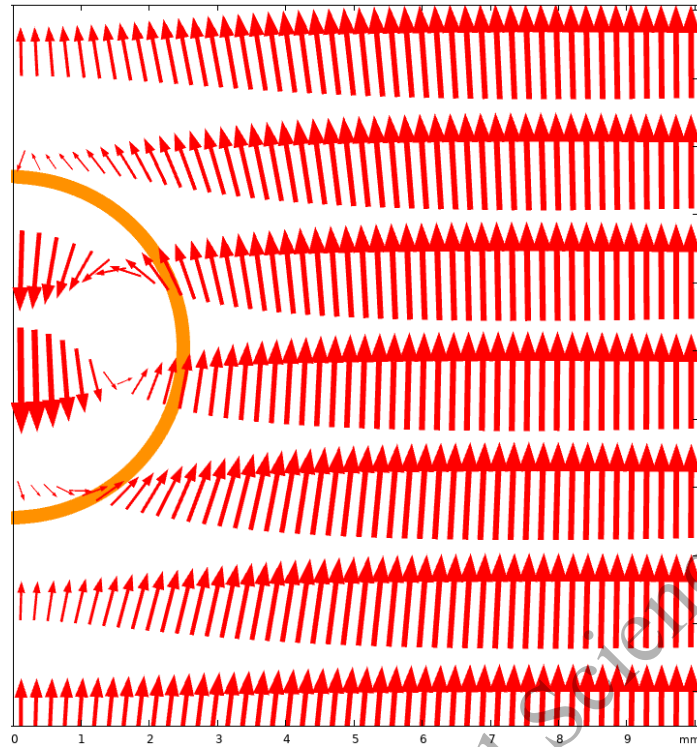
Figure 10.   The speed field of a falling bubble in a measuring cylinder. The length of an arrow is proportional to the speed at its midpoint.

In Figure 10, the arrows represent the velocity of the fluids. For better clarification, the reference point of the velocity field is the uppermost point of the bubble, so the figure looked as if the bubble remained stationary and the outer fluid flows by. The bubble fluid near the interface flows upward along the interface due to the viscous force of the outer fluid, while the bubble fluid near the axis of symmetry flows downward to maintain the conservation of mass.

Only two factors can affect the drag of the liquid bubble: the viscous force the outer fluid exerts on the bubble, and the vortex behind the bubble (not shown on Figure 10, but exists when Re becomes higher.)

1)   The Effect of the Viscosities on the Viscous Force

The Newton's law of viscosity demonstrated that the viscous force depends on the speed gradient, since both fluids are Newtonian fluids:

$$\tau_{y,x} = -\mu \frac{du_x}{dy} \tag{16}$$

Here τ is the shear stress, u_x is the x-component of the velocity of the fluid, and y is the y-coordinate. Therefore, the steeper the speed gradient of the outer fluid near the interface, the stronger the viscous force it exerts on the bubble.

For a rigid bubble, it is straightforward that the speed gradient depends only on the viscosity of the outer fluid and the speed at which the bubble falls. However, the bubble itself is a fluid, and therefore flow exists on the interface of the bubble and inside the bubble. The faster the superficial speed the bubble has, the less speed difference in the boundary layer is, and the less steep the speed gradient of the outer fluid is. Thus, the drag decreases.

Simulation supports that changes in bubble viscosity affects the drag. It shows that the oil bubble fell 23.3% faster (from $78.18\,mm \cdot s^{-1}$ to $96.31\,mm \cdot s^{-1}$) when oil temperature increases from 30℃ to 90℃. (However, the velocities of water bubbles under 30℃ and 90℃ reveal that the bubble's viscosity does not contribute much change to the superficial speed of water bubbles, since water's viscosity changes little in relation to temperature.)

Simulation (see Figure 11) further shows how the viscosity of the bubble affects the speed gradient of both fluids. To magnify the effect of bubble viscosity, it is better to use oil bubbles, whose viscosity changes dramatically with respect to temperature. The simulation involves two rice bran oil bubbles that are under 30℃ (Figure 11(a)) and 90℃ (Figure 11(b)) and fall through two ethanol solutions with densities of $810\mathrm{kg} \cdot m^{-3}$ and $835\mathrm{kg} \cdot m^{-3}$, respectively. The resultant speed of the bubbles is held constant at $78\,mm \cdot s^{-1}$. The reference point of the speed field is the uppermost point of the bubble, still.
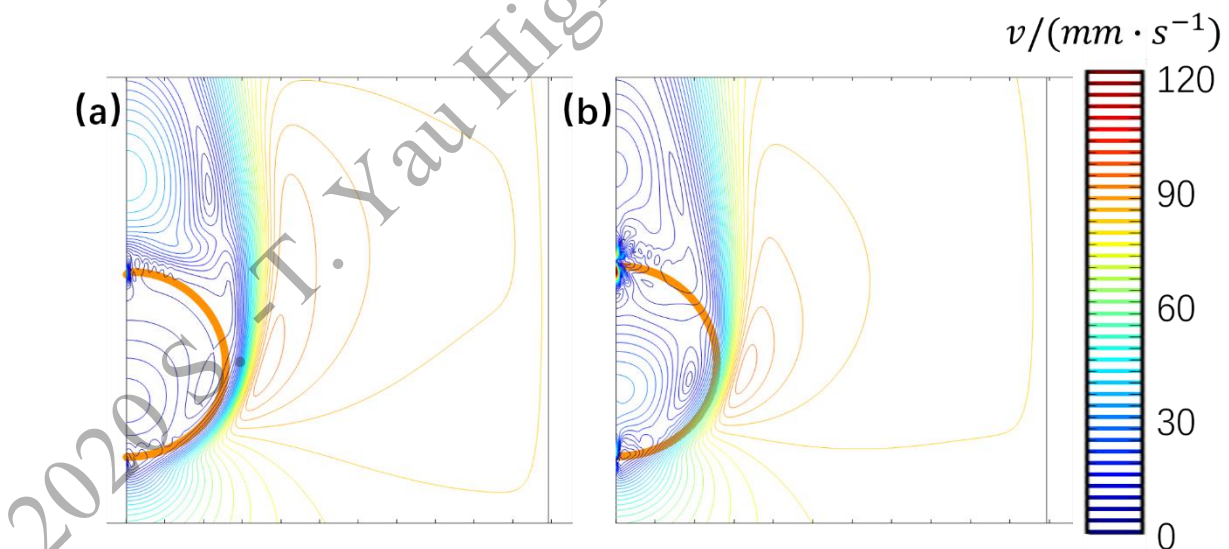

Figure 11.   Two rice bran oil bubbles that are under 30℃ (a) and 90℃ (b) falling through two ethanol solutions with densities of $810\mathrm{kg} \cdot m^{-3}$ and $835\mathrm{kg} \cdot m^{-3}$, respectively, at the same speed of $78\,mm \cdot s^{-1}$. Contour: speed. Interval: $3\,mm \cdot s^{-1}$.

Figure 11 shows that, the less viscous bubble allows a steeper speed gradient inside the bubble, resulting in a higher superficial speed.

In fact, the ratio of the viscosity of the inner fluid to that of the outer fluid is a good approximation of the speed gradient distribution inside and outside the bubble (see Figure 12), suppose that the gradient is linear and the acceleration of the superficial fluid is negligible. In Figure 10, both bubbles have a point where the speed is zero. It is represented by the blue circle in Figure 12. Also, the interface is marked by the blue vertical line. The speed gradient outside the bubble gives the interface a positive viscous force, and the speed gradient inside the bubble gives the interface a negative viscous force. For these two forces to be balanced, the ratio of velocity gradient must be the inverse of the ratio of the viscosity ratio. Thus Equation (10) makes sense.
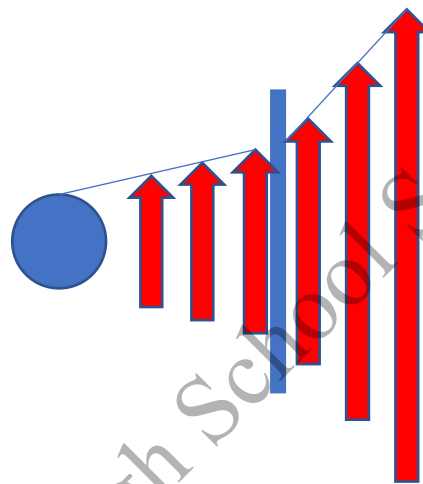

Figure 12.   The speed field inside and near the interface of the bubble. The blue circle is the point where speed is zero (inside the bubble.) The blue line is the interface; the red arrows mark the speed field.

In conclusion, the drag force has a positive causal relationship with both the viscosities of the inner and outer fluids. The ratio between the viscosities can approximate the distribution of speed gradient near the interface, both inside and outside.

2)   The Effect of the Viscosities on the Vortex

The drag of the bubble has a positive causal relationship with the area of vortex behind it. However, as shown in the following discussions, the viscosities of the inner and outer fluids influence the separation point differently.

a) Outer Fluid

When μ increases, the Reynolds number Re decreases. The separation point, which is solely determined by Re, shifts upstream thus.

b) Inner Fluid

A more viscous bubble is more resistant to the flow, flowing with less speed on the interface. This is in equivalent with the outer fluid flowing at a higher speed, which would also

cause an increase in the Reynolds number. Thus, the separation point shifts upstream. This is also supported by the simulation result shown in Figure 11.

c) Conclusion

The viscosities of the bubble and the outer fluid have opposite effects on the separation point. Under the same bubble speed, the separation point moves upstream when the bubble's viscosity increases and the outer fluid's viscosity decreases. Further, when temperature increases, the viscosities of both fluids increase, and the shift of the separation point depends on whose viscosity change is more dominant.

B. Effective Bubble Diameter

Prolong the speed gradient shown in Figure 13, it reaches a surface where the speed is zero, as shown in Figure 13.
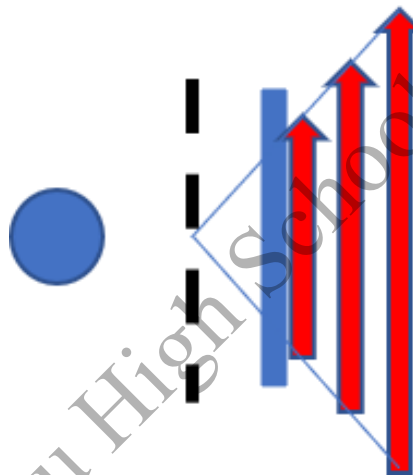

Figure 13.   Prolonged speed gradient. The dashed line is the imaginary surface where the speed is zero.

This is particularly significant because, if the surface of the bubble is moved inwards to the black dashed line, it will have no superficial flow, and therefore it can be regarded as a solid-liquid interface. That is to say, every liquid bubble has a smaller solid equivalent. The diameter of the solid equivalent is defined as the effective bubble diameter, $L_{effective}$. Note that this is a simplified model. In reality, the speed gradient of the outer fluid is not linear, and it is not constant: on the bottom and the top of the bubble, it is less steep.

Another method to find a solid equivalent of a liquid bubble is simply subtracting the superficial speed of the liquid bubble from the speed of the outer fluid. These two methods have different impacts on the flow field:

1)   Decreasing the Diameter

It maintains the speed but decreases the area of vortex behind the bubble. It maintains the speed so it does not change the speed v in Equation (7). Also, as shown in Figure 11, the speed gradient is less steep near the bottom of the bubble, meaning the point with zero speed is further inside the bubble. That is to say, a uniform $L_{effective}$ decreases the viscous force acting on the bubble more than it decreases the viscous force at the bottom of the bubble.

2)   Subtracting the Superficial Speed

It maintains the area of vortex but decreases its speed. It maintains the diameter so it does not change the reference area A in Equation (7). Also, decreasing the speed of the outer fluid lessens the viscous force by roughly the same proportion over all of the interface. Finally, it can wipe out the systematic error in the simulation, if any.

Therefore, a combined method will probably be the most optimal. Both $L_{effective}$ and another constant b are appended to the Equation (15) to obtain Equation (17)

$$3\pi\mu(v-b)\,L_{effective}\left[1 + 0.15\left(\frac{\rho_0(v-b)L_{effective}}{\mu}\right)^{0.687}\right] = \frac{4}{3}\pi\left(\frac{L}{2}\right)^3(\rho-\rho_0)g \ (17)$$

Where $L_{effective}$ is in meters, and b is in meters per second. For better clarification, all variables, including v, are now presented in SI units.

The data in Figure 7 were used to test Equation (17). When $\begin{cases} L_{effective} = 0.0051m \\ b = 0.002m \cdot s^{-1} \end{cases}$, the predicted value accurately described the curve when other parameters were constant: $\begin{cases} \mu = 0.001043Pa \cdot s \\ L = 0.005m \end{cases}$. The result is shown in Figure 14.
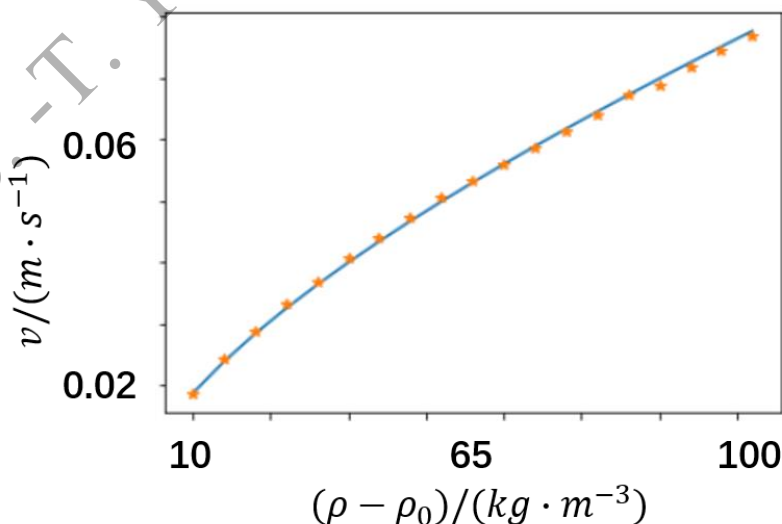

Figure 14.   Simulation results and predicted values (after fitting.) The orange asterisks are the simulation results, and the blue line is the line fitted by Equation (17).

C. Determining $L_{effective}$ and b

1)   The Relationship Between $L_{effective}$ and b

As illustrated, $L_{effective}$ and b are both used to find the solid equivalent of a liquid bubble. Therefore, they should be positively related to each other—when $L_{effective}$ does not increase the bubble speed much, b should be larger to compensate, *vice versa.* To validate this hypothesis, six best-fit lines are drawn. Each line approximates a $v - (\rho - \rho_0)$ curve under a particular μ. Meanwhile, L and ρ are constant: $\begin{cases} L = 0.005m \\ \rho = 900kg \cdot m^{-3} \end{cases}$

To further guarantee the validity and accuracy of the simulation, μ has relatively high values in this investigation, so that Re does not exceed 210. Thus, the vortexes, if any, are always symmetrical and steady, matching the simulation settings.

The results are shown in Table III, and the graphs are shown in Figure 17 in the Appendix. The error bounds are determined when the fitted line clearly visibly diverges from the simulation datapoints (see Figure 18 and Figure 19 in the Appendix.)

TABLE III.   THE RELATIONSHIPS BETWEEN M, $L_{EFFECTIVE}$ AND B

No.	$\mu(Pa \cdot s)$	$L_{effective}(m \pm 0.0001m)$	$b(m \cdot s^{-1} \pm 0.0004m \cdot s^{-1})$
(a)	0.015	0.0032	-0.0016
(b)	0.01	0.0034	-0.001
(c)	0.006	0.00375	0.0003
(d)	0.004	0.0041	0.0017
(e)	0.0035	0.0042	0.0021
(f)	0.0025	0.0045	0.0033

While fitting the line, it was discovered that $L_{effective}$ mainly adjusted the gradient and curvature of the curve, while b shifted the curve (usually upwards.) This matched the analysis that $L_{effective}$ and b transformed the liquid bubble in different ways to approach its solid equivalent. Also, as predicted, $L_{effective}$ is always smaller than the actual L in the table. However, b is not always nonnegative—when $L_{effective}$ increases the bubble speed too much, b has to be smaller to compensate, according to the analysis at the beginning of this section. In

fact, $L_{effective}$ may be larger than L if b compensates the slowing. This is the case in Figure 14. In conclusion, each of $L_{effective}$ and b does not necessarily decrease the drag or increase the settling speed, but together they must increase the settling speed of the bubble.

b is plotted in relation to $L_{effective}$ (see Figure 13), and it is found that the relationship can be approximated by a second-degree polynomial function:

$$b = b_1 L_{effective}^2 + b_2 L_{effective} + b_3 \tag{18}$$

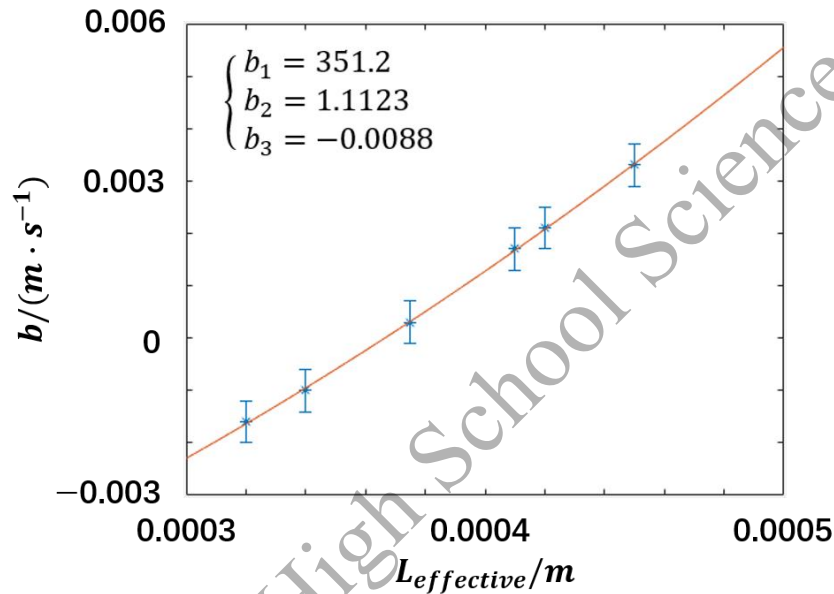The result is graphed in Figure 15.

Figure 15. b for rice bran oil bubbles as a function of $L_{effective}$. Blue asterisks are the simulation results, and the orange line is the line fitted by Equation (18).

2)   The Relationship Between μ and $L_{effective}$

When the bubble viscosity is unchanged, a greater μ makes the bubble viscosity less significant. Therefore, when μ increases, the liquid bubble diverges more from the solid bubble. Thus, it is hypothesized that $L_{effective}$ will decrease if μ increases, *ceteris paribus:*

$$L_{effective} = \frac{k_1}{\mu + k_2} + k_3 \tag{19}$$
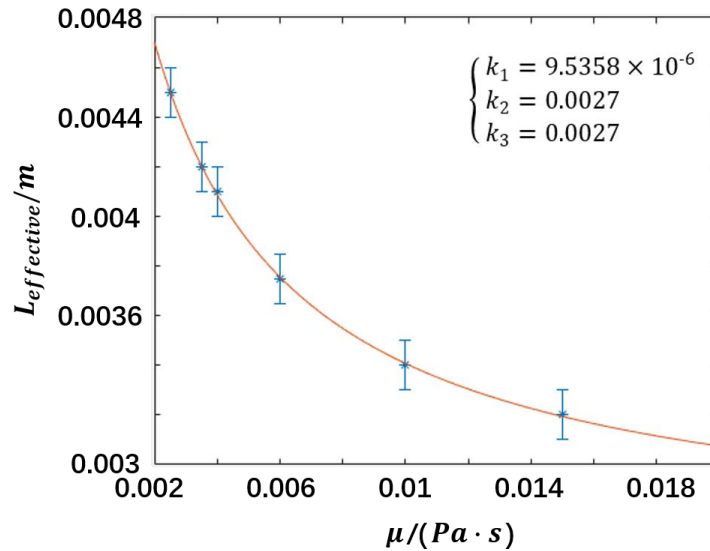
The result is shown in Figure 16.

Figure 16. $L_{effective}$ for rice bran oil bubbles as a function of the viscosity of the outer fluid, μ. Blue asterisks are the simulation results, and the orange line is the line fitted by Equation (19).

According to the equation, $L_{effective}$ would be $0.0062m$ if $\mu = 0$, which somewhat diverges from the actual L of $0.005m$. However, in this case, Re would be infinitely large, and the equation would no longer be applicable.

D. Equations for a Liquid Bubble Falling in Fluid

Substitute Equation (18) and Equation (19) into Equation (15):

$$3\pi\mu\left[v - b_1\left(\frac{k_1}{\mu+k_2}+k_3\right)^2 - b_2\left(\frac{k_1}{\mu+k_2}+k_3\right) - b_3\right]\left(\frac{k_1}{\mu+k_2}+k_3\right)\left\{1 + \right.$$

$$\left.0.15\left[\frac{\rho_0\left[v-b_1\left(\frac{k_1}{\mu+k_2}+k_3\right)^2-b_2\left(\frac{k_1}{\mu+k_2}+k_3\right)-b_3\right]\left(\frac{k_1}{\mu+k_2}+k_3\right)}{\mu}\right]^{0.687}\right\} = \frac{4}{3}\pi\left(\frac{L}{2}\right)^3(\rho-\rho_0)g \qquad (20)$$

Here k_1, k_2, k_3, b_1, b_2, and b_3 depend only on the viscosity and diameter of the bubble. Therefore, they are termed as the "bubble-specific constants." They do not depend on the density of the bubble, ρ, which is already taken into consideration in the equation.

For rice bran oil bubbles at 30℃ (i.e. with a viscosity of $0.057477Pa \cdot s$) and with diameter $5mm$,

$$\begin{cases} k_1 = 9.5358 \times 10^{-6} \\ k_2 = 0.0027 \\ k_3 = 0.0027 \\ b_1 = 351.2 \\ b_2 = 1.1123 \\ b_3 = -0.0088 \end{cases}$$

Equation (20) can be used to deduce the settling speed of a liquid bubble in any other immiscible liquids, when the bubble-specific constants k_1, k_2, k_3, b_1, b_2, and b_3 are given. To measure the unknown bubble-specific parameters, the same steps showed with oil bubbles should be repeated. However, the applicable range of this equation is yet to be investigated. So far, the only discovered restraint is $0.2 < Re < 800$. Moreover, the equations are mainly validated with data with $Re < 210$. Also, the definition of the variables in Re should be reexamined. The modified equation uses $(v - b)$ and $L_{effective}$, rather than v and L, to calculate Re. Finally, although the equation matches the simulation, it is yet to be tested by experiments. Perhaps some further modifications (using other expressions to approximate $L_{effective}$ and b, or adjusting the bubble-specific constants) should be made to the equation.

E. Further Investigations—Eliminating the Bubble-Specific Constants

The bubble-specific constants are sometimes difficult or expensive to obtain, and they increase the inaccuracy in applying the equation and also hinder the utility of it. However, they can potentially be replaced by other variables.

$L_{effective}$ is determined by the viscosity of the outer fluid when the bubble viscosity and diameter are constant. However, what directly impacts $L_{effective}$ is the relationship between bubble viscosity and the viscosity of the outer fluid, rather than the latter itself. Perhaps the ratio of them, along with L, can be used to determine and thus replace k_1, k_2 and k_3 in a way similar to Equation (10). Also, $L_{effective}$ closely relates to the actual diameter of the bubble. L may also be effective in determining the values of the bubble-specific constants.

Due to the complexity of this problem, probably the best way to determine these relationships is by obtaining more data and fitting lines semi-empirically. Due to resource and time restrictions, these further analyses are not included in this article.

V. CONCLUSION

The process of a liquid bubble coming out from a needle and falling through another immiscible liquid was investigated. The experiment used a measuring cylinder with diameter 10.92mm, and oil, ethanol and water as the fluids. The experiment and simulation results were examined, and the conclusions are summarized as follows:

(1) The viscosity curves of oils can be approximated by hyperbolas.

(2) The settling speed of the bubble is positively related with its diameter L, density ρ,

and negatively related with its viscosity and the outer fluid's viscosity μ.

(3) The diameter L of the bubble is positively related with the perimeter of the needle and negatively related to the density difference of the bubble and the outer fluid, $(\rho - \rho_0)$.

(4) The simulation has a systematic error because of the literature value of the viscosity of rice bran oil. But when the oil viscosity is calibrated, or when the viscosities are manually set, the simulation is highly accurate.

(5) An increase in temperature T causes the separation point to shift upstream when the outer fluid viscosity μ is dominant and causes the separation point to shift downstream when the bubble viscosity is dominant. It should be mentioned that, when T increases and the bubble becomes less viscous, although the area of vortex is larger, the decrease in viscous force is more significant, causing the bubble to fall faster.

(6) The equation describing the drag force experienced by a falling solid sphere also applies to liquid bubbles with some modifications. Equations describing the settling velocity of a liquid bubble are derived and shown in details in Equation (18), Equation (19) and Equation (20).

VI. REFERENCES

[1] C. Oseen (1927), Hydrodynamik, Chapter 10, Akademische Verlagsgesellschaft, Leipzig.

[2] S. Goldstein (1929), The Steady Flow of Viscous Fluid Past a Fixed Spherical Obstacle At Small Reynolds Numbers, Proc. R. Soc. Lond. 123A.

[3] A.R. Khan & J.F. Richaedon (1987), The Resistance To Motion Of a Solid Sphere In a Fluid, Chemical Engineering Communications, 62:1-6, 135-150.

[4] Diamante, L. M., & Lan, T. (2014). Absolute viscosities of vegetable oils at different temperatures and shear rate range of 64.5 to 4835 s− 1. Journal of food processing.

[5] Shreya N. Sahasrabudhe, Veronica Rodriguez-Martinez, Meghan. O'Meara & Brian E. Farkas (2017), Density, viscosity, and surface tension of five vegetable oils at elevated temperatures: Measurement and modeling, International Journal of Food Properties, 20:sup2,1965-1981.

[6] Jaber Almedeij (2008), Drag Coefficient of Flow Around a Sphere: Matching Asymptotically the Wide Trend, Powder Technology, Volume 186, Issue 3, 218-223.

[7] Amol A. Kulkarni and Jyeshtharaj B. Joshi (2005), Bubble Formation and Bubble Rise Velocity in Gas−Liquid Systems: A Review, Industrial & Engineering Chemistry Research, 44 (16), 5873-5931.

[8] Schiller L., and Naumann A. (1933), Z. Ver Deut. Ing., 77, 318.

[9] T. A. JOHNSON and V. C. PATEL (1999), Flow past a sphere up to a Reynolds number of 300, Journal of Fluid Mechanics, 378.

VII.   ACKNOWLEDGMENT

VIII. APPENDIX

A. Graphs

1) Table III Fitting Lines

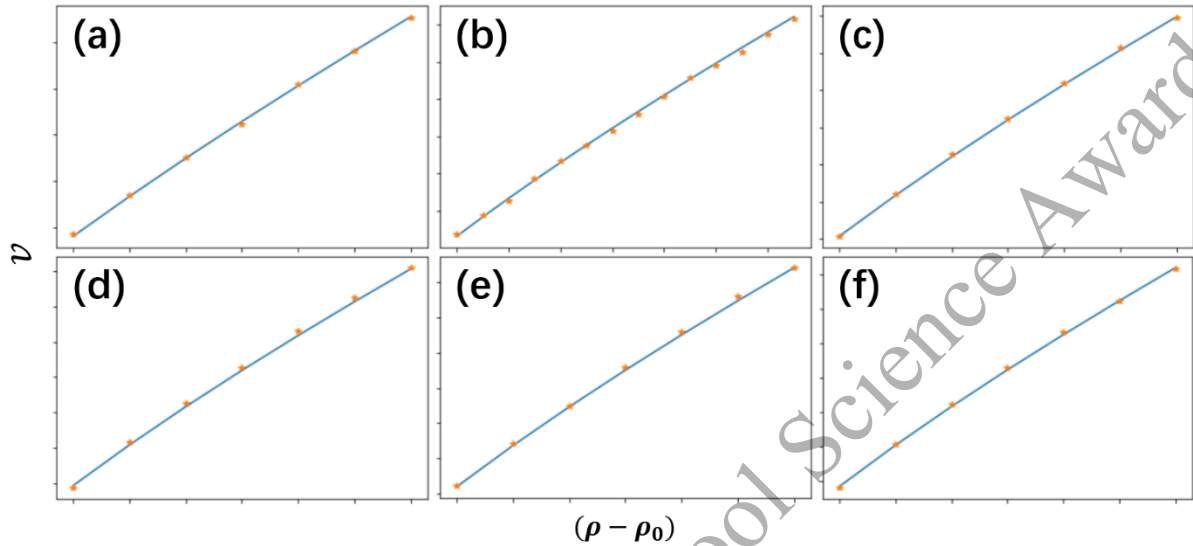Figure 17   shows the fitting results with the parameters in Table III.

Figure 17.   Graphs of Table III. Each graph represents a fitting after tuning the parameters.

2) Table III Error Bounds

a) $L_{effective}$

The fitting results of the simulation in Table III (c) is graphed in Figure 18. When $L_{effective}$ diverges from the best value (0.00375m) by 0.0001m, the diverge in gradient and curvature is clearly visible. Therefore, the error bound for $L_{effective}$ is 0.0001m.

Note that horizontally shifting the curve is the job of b, rather than $L_{effective}$; $L_{effective}$ focuses on adjusting the gradient and curvature of the fitting line.
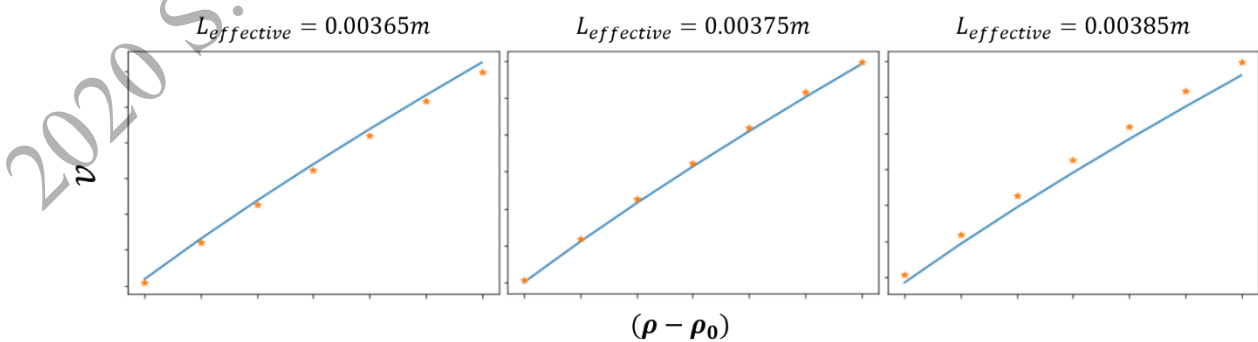

Figure 18.   Fitted lines with different values of $L_{effective}$. When $L_{effective}$ diverges from the best value (0.00375m) by 0.0001m, the diverge in gradient and curvature is clearly visible.

b) b

The fitting results of the simulation in Table III (c) is graphed in Figure 19. When b diverges from the best value ($0.0003 \text{m} \cdot \text{s}^{-1}$) by $0.0004 \text{m} \cdot \text{s}^{-1}$, the error is clearly visible. Therefore, the error bound for b is $0.0004 \text{m} \cdot \text{s}^{-1}$.
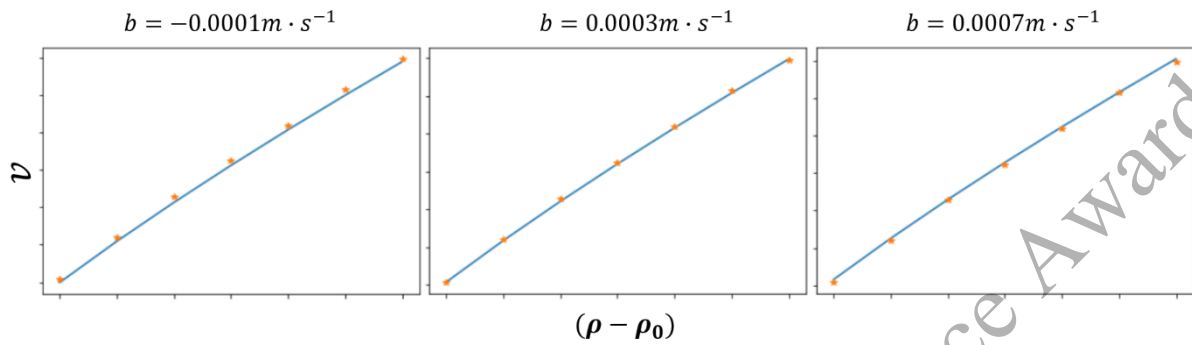

Figure 19.   Fitted lines with different values of b. When b diverges from the best value ($0.0003 \text{m} \cdot \text{s}^{-1}$) by $0.0004 \text{m} \cdot \text{s}^{-1}$, the error is clearly visible.